Published OnlineFirst August 11, 2009; DOI: 10.1158/1535-7163.MCT-08-1203

Three-kinase inhibitor combination recreates multipathway effects of a geldanamycin analogue on hepatocellular carcinoma cell death

Justin R. Pritchard,[1] Benjamin D. Cosgrove,[2] Michael T. Hemann,[1] Linda G. Griffith,[2] Jack R. Wands,[3] and Douglas A. Lauffenburger[1,2]

Departments of [1]Biology and [2]Biological Engineering, Massachusetts Institute of Technology, Cambridge, Massachusetts and [3]The Warren Alpert Medical School of Brown University, Providence, Rhode Island

Abstract

Multitarget compounds that act on a diverse set of regulatory pathways are emerging as a therapeutic approach for a variety of cancers. Toward a more specified use of this approach, we hypothesize that the desired efficacy can be recreated in terms of a particular combination of relatively more specific (i.e., ostensibly single target) compounds. We test this hypothesis for the geldanamycin analogue 17-Allylamino-17-demethoxygeldanamycin (17AAG) in hepatocellular carcinoma cells, measuring critical phosphorylation levels that indicate the kinase pathway effects correlating with apoptotic responsiveness of the Hep3B cell line in contrast to the apoptotic resistance of the Huh7 cell line. A principal components analysis (PCA) constructed from time course measurements of seven phosphoprotein signaling levels identified modulation of the AKT, IκB kinase, and signal transducer and activator of transcription 3 pathways by 17AAG treatment as most important for distinguishing these cell-specific death responses. The analysis correctly suggested from 17AAG-induced effects on these phosphoprotein levels that the FOCUS cell line would show apoptotic responsiveness similarly to Hep3B. The PCA also guided the inhibition of three critical pathways and rendered Huh7 cells responsive to 17AAG. Strikingly, in all three hepatocellular carcinoma lines, the three-inhibitor combination alone exhibited similar or greater efficacy to 17AAG. We conclude that (*a*) the PCA captures and clusters the multipathway phosphoprotein time courses with respect to their 17AAG-induced apoptotic responsiveness and (*b*) we can recreate, in a more specified manner, the cellular responses of a prospective multitarget cancer therapeutic. [Mol Cancer Ther 2009;8(8):2183–92]

Introduction

The fairly limited success of many targeted cancer therapeutics when used as single-agent treatments presents a challenging problem that has motivated studies seeking to stratify failure-versus-success categories (1) or to combine targeted therapeutics with traditional chemotherapeutic regimens (2). An alternative avenue generating growing interest is a new class of compounds known as multitarget drugs (3). These compounds aim to improve therapeutic efficacy by producing a combined inhibition of diverse regulatory pathways that are important for cancer cell proliferation and survival.

At one end of the multitarget drug spectrum lies a class of Hsp90 inhibitors, such as 17-allylamino-17-demethoxygeldanamycin (17AAG), which were derived from the tumoricidal natural product geldanamycin (4). Hsp90 is a vital chaperone that, relative to other chaperones, interacts with a select but critical subset of cellular proteins, including nuclear hormone receptors and components of signal transduction cascades (5). Hsp90 inhibition seems to offer a promising anticancer strategy (6) but, compared with more traditional targeted therapeutics, an exceptionally pleiotropic effect. In a recent genome-wide study in *Saccharomyces cerevisiae*, Hsp90 was found to interact with ~10% of the open reading frames investigated (7).

The nature of the effects of 17AAG in tumor cells relative to nontransformed cells seems to derive from the enhanced binding of 17AAG to Hsp90 in the former. Tumor cell Hsp90 is found more highly resident in multichaperone complexes with high rates of ATPase activity, constituting a distinctive molecular state exhibiting an ~10-fold greater binding affinity for 17AAG compared with that in the normal cells (8). Hsp90 inhibition in a variety of tumor cell lines has been shown to affect the levels and/or activity of ErbB family receptors, Src, Ras, Raf, AKT, IκB kinase (IKK), Janus kinase, Her2, p53, RIP, and cell cycle regulators, as well as increasing the levels of the antiapoptotic chaperone Hsp70 (5, 9–14). In addition to these long-term effects on client protein levels and their associated downstream signaling effects, short-term effects of Hsp90 inhibitors have also been observed.

Received 12/22/08; ` revised 4/9/09; accepted 6/1/09; published OnlineFirst 8/11/09.

Grant support: NIH training grant (Department of Biology, Massachusetts Institute of Technology), Massachusetts Institute of Technology Presidential Fellowship (J.R. Pritchard), National Cancer Institute Integrative Cancer Biology Program, National Institute of General Medical Sciences Cell Decision Processes Center, and Department of Defense Institute for Collaborative Biotechnologies.

The costs of publication of this article were defrayed in part by the payment of page charges. This article must therefore be hereby marked *advertisement* in accordance with 18 U.S.C. Section 1734 solely to indicate this fact.

Note: Supplementary material for this article is available at Molecular Cancer Therapeutics Online (http://mct.aacrjournals.org/).

Requests for reprints: Douglas A. Lauffenburger, Department of Biological Engineering, Massachusetts Institute of Technology, 77 Massachusetts Avenue, Cambridge, MA 02139. Phone: 617-2521629; Fax: 617-2580204. E-mail: lauffen@mit.edu

doi:10.1158/1535-7163.MCT-08-1203

Published OnlineFirst August 11, 2009; DOI: 10.1158/1535-7163.MCT-08-1203

Geldanamycin treatment has been found to yield increased phosphorylation of AKT in myocytes (15), increased PKR activity and phosphorylation of eIF-2α in HeLa cells (16), and transient early signaling in the Src, AKT, and extracellular signal-regulated kinase (ERK) pathways in both MCF-7 and COS7 cells (17). However, the contributions of these various pathway effects to cell death responses are unclear, and the manner by which these effects integrate to affect cell behavior is even more difficult to ascertain.

Our goal is to offer an effective approach based on systematically extracting the critical effects of multitarget compounds, which could enable the rational recreation of their effectiveness via designed combinations of more selectively targeted drugs. Because Hsp90 inhibition elicits contradictory effects, the degradation of proteins involved in cellular survival as well as an increase in Hsp70 levels, we reason that a rational recreation of its proapoptotic effects may potentially increase efficacy. Our approach is motivated by recent successes in computational characterization of the effects of diverse drug-induced perturbations governing cellular phenotypes (18, 19). Data-driven computational modeling techniques, such as principal components analysis (PCA) and partial least-square regression, seek to find key vectors representing signal combinations that contain the most vital information for predicting—at least in correlative fashion—cell responses to various stimuli (19).

We test this hypothesis on quantitative experimental measurement of multiple phosphoprotein signaling pathways altered by 17AAG in a set of hepatocellular carcinoma (HCC) cell lines. A PCA of time course data for seven kinase signals reveals that early effects of 17AAG on the AKT, IKK, and signal transducer and activator of transcription 3 (STAT3) pathways are predominantly critical for clustering cell-specific apoptotic death responses among the Hep3B, Huh7, and FOCUS lines. Whereas individual inhibition of each of these three pathways had little effect on the cell responses, combining all three kinase inhibitors rendered the 17AAG-resistant Huh7 line responsive and had greater efficacy than 17AAG itself in two of our three cell lines.

Materials and Methods

Cell Lines and Culture

Hep3B, Huh7, and FOCUS cell lines (20) were obtained from the Wands Lab (Brown University, Providence, RI). Cells were maintained in MEM (American Type Culture Collection) with 10% fetal bovine serum (HyClone) at subconfluent densities and 37°C, 5% CO_2. Apoptosis and signaling experiments were seeded at cell densities of 200,000 and 150,000 cells per well of a six-well plate for Hep3B and Huh7/FOCUS cell lines, respectively.

Inhibitors

All inhibitors were purchased from Calbiochem. 17AAG was reconstituted in methanol; all other compounds [BMS-345541, Janus-activated kinase (JAK) inhibitor 1, pyridone 6, and PI103] were reconstituted in DMSO. PD98059 (Calbiochem) reconstituted in DMSO is the mitogen-activated protein kinase/ERK kinase (MEK) inhibitor used in the control combination study (Supplementary Fig. S2), and the c-Jun NH_2-terminal kinase (JNK) inhibitor is SP600125 (Calbiochem).

Signaling Measurements

Signaling measurements were made using bead-based ELISA kits manufactured by Bio-Rad. Bioplex assays were run according to all of the manufacturer's recommendations. These Bioplex assays were used to measure phospho-AKT (Ser^{473}), phospho-ERK1/2 (Thr^{202}/Tyr^{204}), phospho-STAT3 (Tyr^{705}), phospho-p38 (Thr^{180}/Tyr^{182}), phospho-JNK (Thr^{183}/Tyr^{185}), phospho–glycogen synthase kinase-3α/β (GSK-3α/β; Ser^{21}/Ser^{9}), phospho–IκB-α (Ser^{32}), AKT, p38, and ERK. All measurements are the mean of duplicates. Measurements were taken at 0, 1, 2, 4, and 24 h after addition of 1 μmol/L 17AAG and normalized to unstimulated controls on a cell line by cell line basis. This fold change normalization created a relative value of 1 for all signals in all cell lines at the point of 17AAG addition. This allowed direct comparison of the fold change of 17AAG effects across cell lines.

Apoptosis Assays

Cells were harvested from six-well plates and combined with the floating fraction. This sample was fixed in 3% to 4% paraformaldehyde and then permeabilized for antibody staining in methanol and stored at −20°C for up to 1 wk. Cells were stained with antibodies for cleaved (activated) caspase-3 (BD Pharmingen) and cleaved poly(ADP-ribose) polymerase (PARP; BD Pharmingen) at a dilution of 1:300 (in PBS-0.1% Tween 20-1% bovine serum albumin). Secondary antibodies were IgG Alexa Flour 647 and Alexa Fluor 488 (Invitrogen) at 1:300 in PBS-0.1% Tween 20-1% bovine serum albumin. A minimum of 10,000 gated events was collected per sample. All measurements are the mean of triplicates ± SE.

Data Analysis

PCA (21) was done using Simca-p++ v11.5 (22). All signals were mean centered and unit variance scaled before analysis. This centering and scaling allows all signaling variables to be considered on an equal scale in principal components space based solely on induced variation relative to the mean of a given signal and its position in the distribution. PCA finds directions of covariance in the original data set. These directions become the principal components onto which the original data set is collapsed. Our initial multidimensional data are condensed down into two principal components dimensions that capture the majority of the variance. Loadings plots are created by plotting the original time dimension in the two-component graph. Scores plots are generated by plotting the original signaling data in the two-component plot. Hotelling's criterion displays the distance in the model plane at which a given sample is behaving significantly different than the rest of the data with 95% confidence (23). For an intuitive description of PCA, see Supplementary Fig. S1. In our data set, we use a variation of principal components cluster analysis. Because all of our signaling variables cannot be segmented into completely separable groups, we use a "dissection-based" or "segmentation-based" technique (21). Here, we calculate a

Published OnlineFirst August 11, 2009; DOI: 10.1158/1535-7163.MCT-08-1203

Euclidean distance based on the original variables (a contribution vector) to identify signals that are the most distinct between sensitive and resistant cell lines.

The appropriate threshold to interpret the PCA was decided on by the small increase in goodness of fit that was provided by a third component. To determine whether the percentage of the cumulative variance explained by our model was significant, we generated 1,000 data matrices of the same size as our original data set. The data matrix entries were found by randomly sampling the column indices across a signaling row. This perturbation retains similar variance structure to the original signal. Our test statistic was the cumulative percentage of the variance explained by a two-component model built in Matlab v7.0 (using the princomp.m function) on these 1,000 data matrices. The test statistic was then plotted as a histogram, a normal distribution was fit to the data, and a *P* value was calculated using the cumulative distribution function.

Integrals (0–4 h) were calculated using a second-order polynomial curve fit followed by numerical integration using a 0.2-h increment. Heat maps were made in Matlab v7.0. The analysis of synergy was coded using Matlab. Statistical comparisons of cell death were done using a Student's *t* test. *P* values of <0.05 were deemed significant.

Results

Conventional Markers of 17AAG Action Cannot Account for the Differential Cell Death Responses in Huh7 and Hep3B Cells

The effect of 17AAG treatment on cell death in HCC cell lines was assessed by treating Huh7 and Hep3B with 17AAG at 0.1 and 1 μmol/L for 48 hours. A representative gating for a population staining double positive for active (cleaved) caspase-3 and cleaved PARP was assessed via flow cytometry (Fig. 1A). Double-positive cells represent the population of cells within a well that are undergoing apoptosis. The same gating thresholds were used for all of the samples from a given cell line and are based on the negative control. No single positive populations were noted at 48 hours during the duration of our study. Three samples per cell line/condition were averaged using the values obtained from the plots in Fig. 1A and are plotted in Fig. 1B. Hep3B cells were found to be sensitive to 1 μmol/L 17AAG–induced cell death, whereas Huh7 cells were found to be resistant (Fig. 1B). We then hypothesized that a difference in the levels of phospho-AKT (Ser^{473}), total AKT, phospho-ERK1/2 (Thr^{202}/Tyr^{204}), and phospho–IκB-α (Ser^{32}/Ser^{36}) 24 hours after the addition of 17AAG might account for the difference in phenotype (Fig. 1C). Lysates were collected both before and 24 hours after treatment with 17AAG. The relative decrease in these four measurements at 24 hours is identical in sensitive and resistant cell lines. These late-time measurements indicate that a simple explanation about the long-term signaling degradation arising from 17AAG treatment is not able to explain the disparate death responses of Hep3B and Huh7 cells.

A Dynamic Multipathway Analysis Can Distinguish Huh7 Resistance and Hep3B Sensitivity to 17AAG

Because the degradation of phosphatidylinositol 3-kinase (PI3K)-AKT, Ras/Raf/MEK/ERK, and IKK-NF-κB pathway signaling at 24 hours failed to distinguish Huh7 from Hep3B, we proposed that a dynamic study including measurements of the shorter-term effects of 17AAG treatment might yield information that could distinguish the differential response behaviors of these cell lines. We thus measured the levels of the same signals at 0, 1, 2, 4, and 24 hours after treatment in both the Huh7 and Hep3B cells. These time points were initially chosen based on the literature reports of early and late changes in phosphorylation levels in response to 17AAG (17). These measurements were normalized to an untreated control for each cell line and are plotted in Fig. 2A as fold change induced by 17AAG. Both Huh7 and Hep3B exhibited transient early phospho-JNK activation. However, relatively stronger transient activation and/or relatively weaker degradation were seen for most other signals (phospho-AKT, phospho–IκB-α, phospho–GSK-3α/β, phospho-ERK1/2, phospho-p38, and phospho-STAT3) in Huh7 cells compared with Hep3B cells (Fig. 2A). Strikingly, the integrated signal changes over the first 4 hours after 17AAG treatment are higher across many components in Huh7 cells than in Hep3B cells (Fig. 2B). To more effectively interpret these data, we used PCA, a technique that models multivariate data in terms of key combinations of measurements exhibiting major covariation in the data set. These combinations can be viewed geometrically as "directions" (or vectors) in the "space" of the signaling measurements defined by axes representing a combination of the measured time points and the integral metric. The direction of greatest covariation (an axis representing the time points that are most similar), which incorporates the most important measurement combinations, is the principal component 1 (PC1); principal component 2 (PC2) then incorporates the next most important measurement combinations best capturing the residual covariation, and so on. The principal components collapse the original multidimensional data into a reduced number of axes representing the most important underlying variables. In our case viewing a "loadings plot" (data summarized in Fig. 3C), the six dimensional data sets (1 hour, 2 hours, 4 hours, 24 hours, and early/late integral metrics) can be comprehended in two-dimensional principal components space as early signaling (representing primarily 1 hour, 2 hours, and the early integral data; PC1) and late signaling(where the 24-hour data project most strongly; PC2). These underlying variables are just combinations of the original variables that best comprehend the data within the entire signaling measurement "vector space" (Supplementary Fig. S1 offers an illustrative tutorial). Our model with two principal components effectively captures 91% of the cumulative variance. Our cutoff was readily established by the major drop in the variance captured by the third component (Fig. 3A). Furthermore, a resampling of our data set determined that our analysis captures significantly ($P = 0.0002$) greater variance than one can capture with 1,000 two-component models

Published OnlineFirst August 11, 2009; DOI: 10.1158/1535-7163.MCT-08-1203

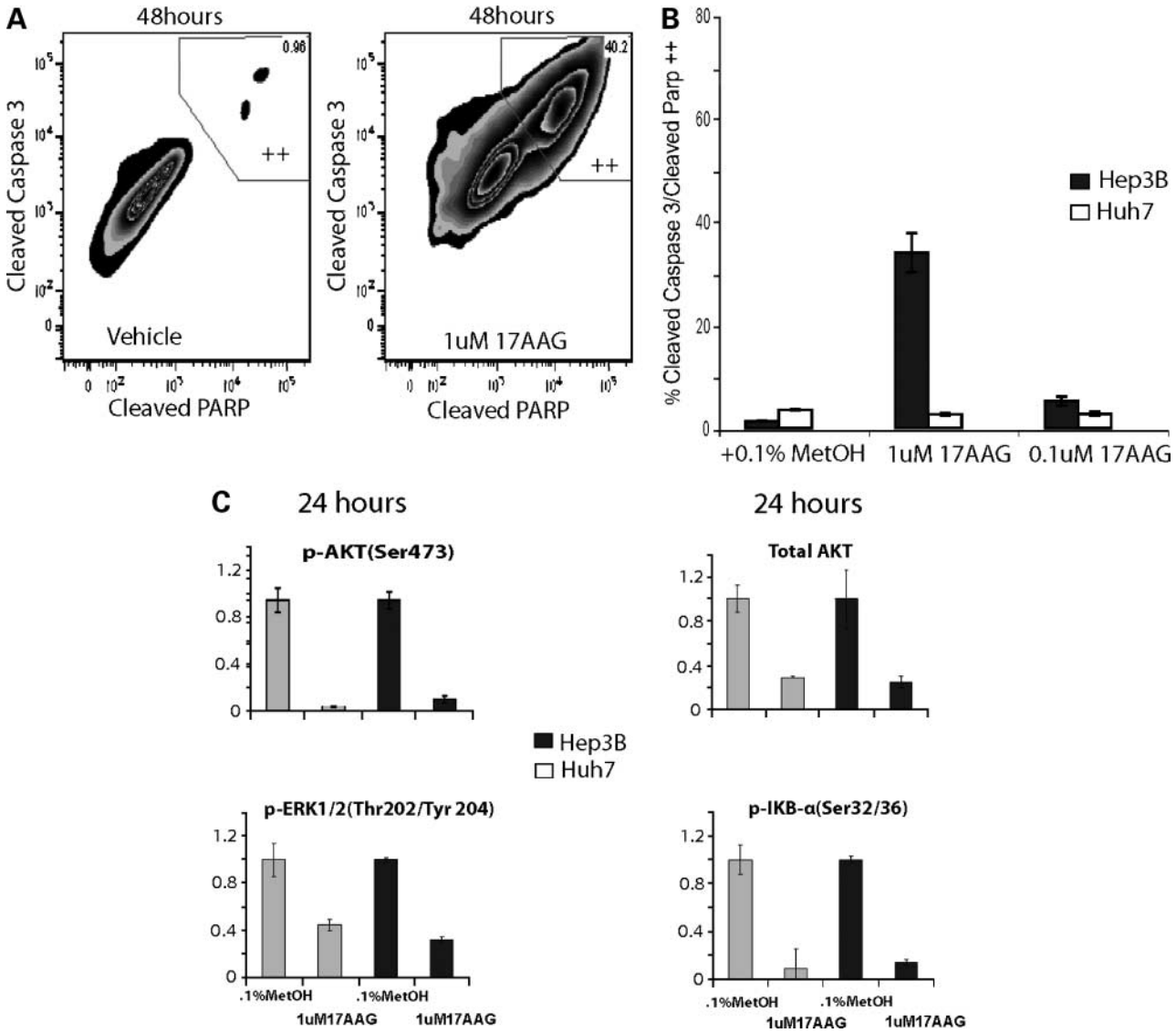

Figure 1. A plot for the cleaved caspase-3/cleaved PARP double-positive population at 48 h measures the susceptibility of Hep3B and the resistance of Huh7 cells to 17AAG. Typical measurements of 24-h signaling degradation in response to 17AAG fail to correlate with this distinction. **A,** a representative flow cytometry scatter plot depicts Hep3B-fixed and Hep3B-permeabilized cells that are stained with antibodies for active cleaved caspase-3 and cleaved PARP at 48 h after treatment with 1 μmol/L 17AAG or 0.1% methanol vehicle control. The double-positive population is denoted by the gating in the upper right-hand corner. Different gatings were used for Huh7 and Hep3B but the scatter plots looked very similar. **B,** the average size of the population of three replicates (±SE) of Hep3B and Huh7 cells as gated in **A** represents the percentage of double-positive apoptotic cells at 48 h ± SE. **C,** late time signals do not correlate with 17AAG susceptibility. Measured at 24 h, the fold change of the mean of duplicates ± SE, treated with 1 μmol/L 17AAG, is normalized to a 0.1% methanol control. Phospho-AKT (Ser^{473}), total AKT, phospho-ERK1/2 (Thr^{202}/Tyr^{204}), and phospho–IκB-α (Ser^{32}/Ser^{36}) were measured by a bead-based Bio-Rad phosphoprotein (Bioplex) assay.

generated by randomly sampling the column index of the rows in our data set (Fig. 3B). Our analysis visually distinguishes the behavior of both Huh7 and Hep3B cells. A so-called "scores plot," in which the various signaling measurements are projected on the principal components axes, visualizes distinct regions where Huh7 signals reside differentially with respect to Hep3B signals (Fig. 3C). These differences are quantified in Fig. 3D, in terms of "contributions vectors," which quantify the disparities between cell line–specific signals (in units of SD) relative to the average distance between all of the signals of the distinct cell lines. The calculated contributions vectors reveal that of the 10 signaling measurements made at each of 5 time points, the most important differences between the drug-resistant Huh7 and drug-sensitive Hep3B lie in the early time points of four signals: phospho-AKT, phospho–IκB-α, phospho-STAT3, and phospho-p38. Because the experimental conditions for the elucidation of the signaling effects grow very rapidly with

Published OnlineFirst August 11, 2009; DOI: 10.1158/1535-7163.MCT-08-1203

the size of the hit set, the phospho-p38 signaling measurements were excluded from further analysis because they reside as an outlier beyond the region of Hotelling's criterion (23) and presented no clear biological hypothesis.

The Principal Components Model Accurately Maps Another 17AAG-Sensitive HCC Cell Line, FOCUS, to the Same Region as Hep3B

To test our PCA, we used our previous approach in a third HCC cell line. A signaling time course for FOCUS cells, analogous to Fig. 2A, shows signal degradation and no transient activation (Fig. 4B). Although certain signaling network differences between FOCUS and Hep3B signaling are evident by inspection, our PCA shows that the FOCUS cells cluster in the same region as the similarly 17AAG-sensitive Hep3B cells (Fig. 4C). Indeed, we found that FOCUS cells are sensitive to 1 μmol/L 17AAG–induced cell death at 48 hours (Fig. 4A). This result shows that the principal components capture critical signal combinations associated with these cell death-versus-survival outcomes.

A Drug Combination Pretreatment Based on Inhibition of Three Key Nodes Partially Sensitizes Huh7 to 17AAG

In Fig. 3D, we identified four signals (phospho-AKT, phospho–IκB-α, phospho-STAT3, and phospho-p38) to be most important in distinguishing Huh7 from Hep3B. We proposed to test whether a combination of drugs inhibiting these key signals in particular could recreate the 17AAG treatment responses. We selected phospho-AKT, phospho-STAT3, and phospho–IκB-α for this purpose, omitting phospho-p38 due to its notification by Hotelling's outlier criteria at a 95% confidence level (23). Pretreatment of Huh7 cells for 12 hours with targeted inhibitors of phospho-AKT (PI3K inhibitor, PI103, 5 μmol/L), phospho-STAT3 (JAK inhibitor 1, pyridone 6, 3 μmol/L; Calbiochem), and phospho–IκB-α (IKK inhibitor, BMS-345541, 15 μmol/L) signaling failed to sensitize Huh7 cells to 1 μmol/L 17AAG at 48 hours (Fig. 5A). However, a combination pretreatment using all three inhibitors together sensitized ($P < 0.0001$) Huh7 cells to 17AAG-induced cell death (Fig. 5A). Moreover, this inhibitor combination induced Huh7 cell death to a significantly greater ($P < 0.0005$) degree than did 17AAG (Fig. 5A). To control for the possibility that any combination of three inhibitors can potentiate 17AAG-induced cell death, inhibition of one critical signal (phospho-STAT3) was combined with inhibition of two noncritical signals (phospho-JNK and phospho-ERK; Fig. 3D). This control drug combination, comprising 3 μmol/L of the JAK inhibitor, 10 μmol/L of a MEK inhibitor (PD98059), and 10 μmol/L of a JNK inhibitor (SP600125), failed to sensitize Huh7 to 17AAG or induce cell death on its own at 48 hours (Supplementary Fig. S2).

Decoupling Proapoptotic Effects from the Overall Context of 17AAG Treatment Creates a Three-Kinase Inhibitor Combination That Works as Well or Better than 17AAG in All Cell Lines

17AAG is known to have both proapoptotic and antiapoptotic effects. Assuming that 17AAG induces cell death through a combination of the proapoptotic consequences of the degradation of key signaling pathway nodes, we hypothesized that the previously identified critical nodes distinguishing sensitive and resistant cells could be key sites for selectively targeted drug contributions in sensitive cells. To test this idea, FOCUS and Hep3B cells were pretreated with the three-kinase drug combination, or control vehicle, for 12 hours before addition of 1 μmol/L 17AAG. The drug combination enhanced 17AAG-induced cell death significantly ($P = 0.050$ and $P < 0.0001$, respectively) in both cases (Fig. 5B). Yet, more strikingly, the drug combination by itself induced cell death as strongly—or more so—than 17AAG in all HCC cell lines. FOCUS cells showed no significant difference between 17AAG and the drug combination–induced cell death, whereas in Hep3B and Huh7 cells the drug combination at 48 hours worked significantly better than 17AAG (Fig. 5A and B).

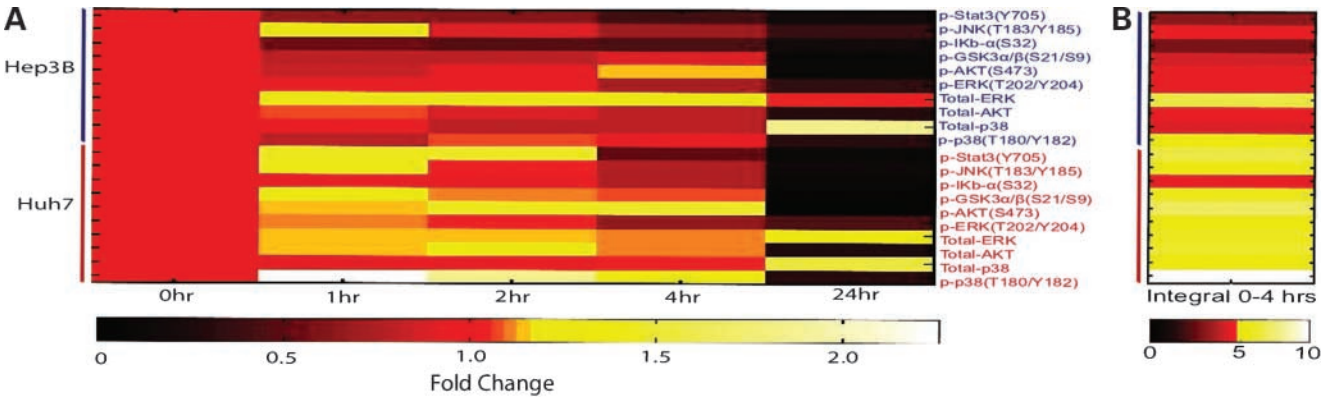

Figure 2. A dynamic signaling time course reveals differences between Hep3B and Huh7. **A,** a signaling time course in Hep3B and Huh7 cells depicts mean fold changes in phosphoprotein signaling in response to 1 μmol/L 17AAG relative to the vehicle only (0.1% methanol) control. **B,** the integral (discussed in Materials and Methods) from 0 to 4 h of 17AAG-induced signaling shows large cumulative differences in early signaling between Huh7 and Hep3B cells.

Published OnlineFirst August 11, 2009; DOI: 10.1158/1535-7163.MCT-08-1203

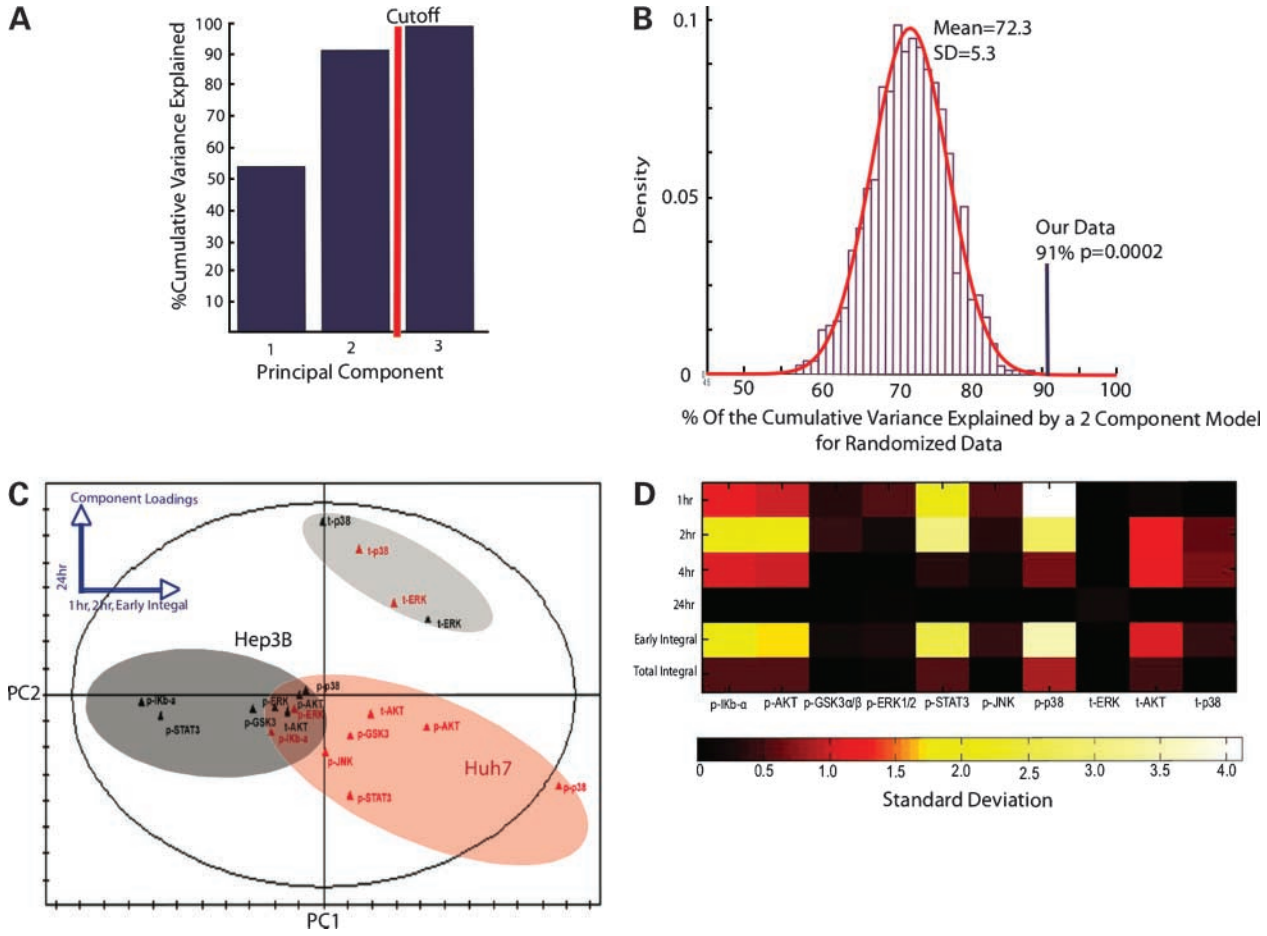

Figure 3. A PCA reduces data complexity and provides testable hypotheses. **A,** percentage of the total variance captured by a model consisting of one, two, or three principal components. There is a marginal increase in the benefit of including principal component 3, indicating an obvious cutoff criterion. **B,** percentage of total variance explained by two-component models that are built on 1,000 perturbed data matrices (see Materials and Methods). A histogram plots the data from the empirical 1,000 matrix sampling. A normal distribution was fit to the histogram data, and our model fit was calculated to have a highly significant *P* value of 0.0002. **C,** a PCA yielded a two-component model that accurately explains 91% of the cumulative variance. PC1 strongly captures variation at early time points and in the 0- to 4-h integral metric. PC2 captures variation at 24 h. These results from the loadings plot are summarized in the upper right-hand corner of the plot. The ellipse represents Hotelling's outlier criteria at a 95% confidence level. The original signaling measurements are plotted in the principal components space. PC1 visually seems to capture cell line variation. The colored ellipses are simply a visualization tool used to bring the readers attention to the distinct clusters in the scores plot. **D,** contributions vectors describe how signals vary in principal components space and are derived computationally by measuring the latent variable distance in terms of the Euclidean distance of the measured variables between Huh7 and Hep3B for a given signal and then comparing that distance to an average distance of all the distances between the cell lines (in units of SD). This plot asks the question of how distinct are two signals between Huh7 and Hep3B cells relative to the average distance between lines. Quantitatively, **D** affirms qualitative observations made in **C**.

Decoupling the Proapoptotic Effects from Their 17AAG Context Allows for Cell Line–Specific Tuning of the Therapeutic Strategy

After finding a drug combination that works as well or better than 17AAG, we wanted to test two hypotheses. First, that the decoupling of a specific pathway effect from the context of 17AAG allows for cell line–specific therapeutic strategies, and second, that the presence of additivity or synergy correlates with cell line–specific differences in the combination inhibitor efficacy relative to 17AAG. To address these questions, we undertook a set of experiments in a JAK inhibitor background, across a 4 × 4 matrix of PI3K and IKK inhibitor concentration combinations, covering four concentrations of each (0, low, medium, and high; Fig. 6). Inspection of the cell death responses reported in this matrix indicated distinct responses for the three cell lines tested. FOCUS cells seemed to primarily be sensitive to the IKK inhibitor in the JAK inhibitor background, whereas Hep3B and Huh7 cells exhibited sensitivity to both IKK and PI3K inhibition (Fig. 6A). Calculation of the fold increase in cell death of a double-drugged entry in the 4 × 4 dosing matrix relative to linear additivity shows that only Huh7 cells exhibit a drug combination synergy (Fig. 6B). This finding of multidrug nonlinear synergy in the Huh7 and multidrug additivity in Hep3B but not FOCUS cells correlates with our observation that the

Published OnlineFirst August 11, 2009; DOI: 10.1158/1535-7163.MCT-08-1203

kinase inhibitor combination could essentially duplicate the 17AAG effects on cell death in the latter, whereas it could exceed the 17AAG effects on cell death in the former two.

Discussion

Inhibition of the Hsp90 chaperone represents a prominent example of a highly complex multitarget therapeutic approach to cancer (5), and studies have explored the myriad of regulatory pathway alterations associated with its effects (5, 9–17). Although these studies have unveiled short-term and/or long-term changes in levels and/or activities of numerous cellular components with opposing effects on the downstream phenotype, there is currently inadequate understanding of pathway alterations that can recapitulate drug efficacy. Our effort here aims to gain quantitative understanding of the key kinase signals underlying the effects of the geldanamycin analogue 17AAG on differential apoptotic death responses of three HCC cell lines: Hep3B, FOCUS, and Huh7. Our studies centered on

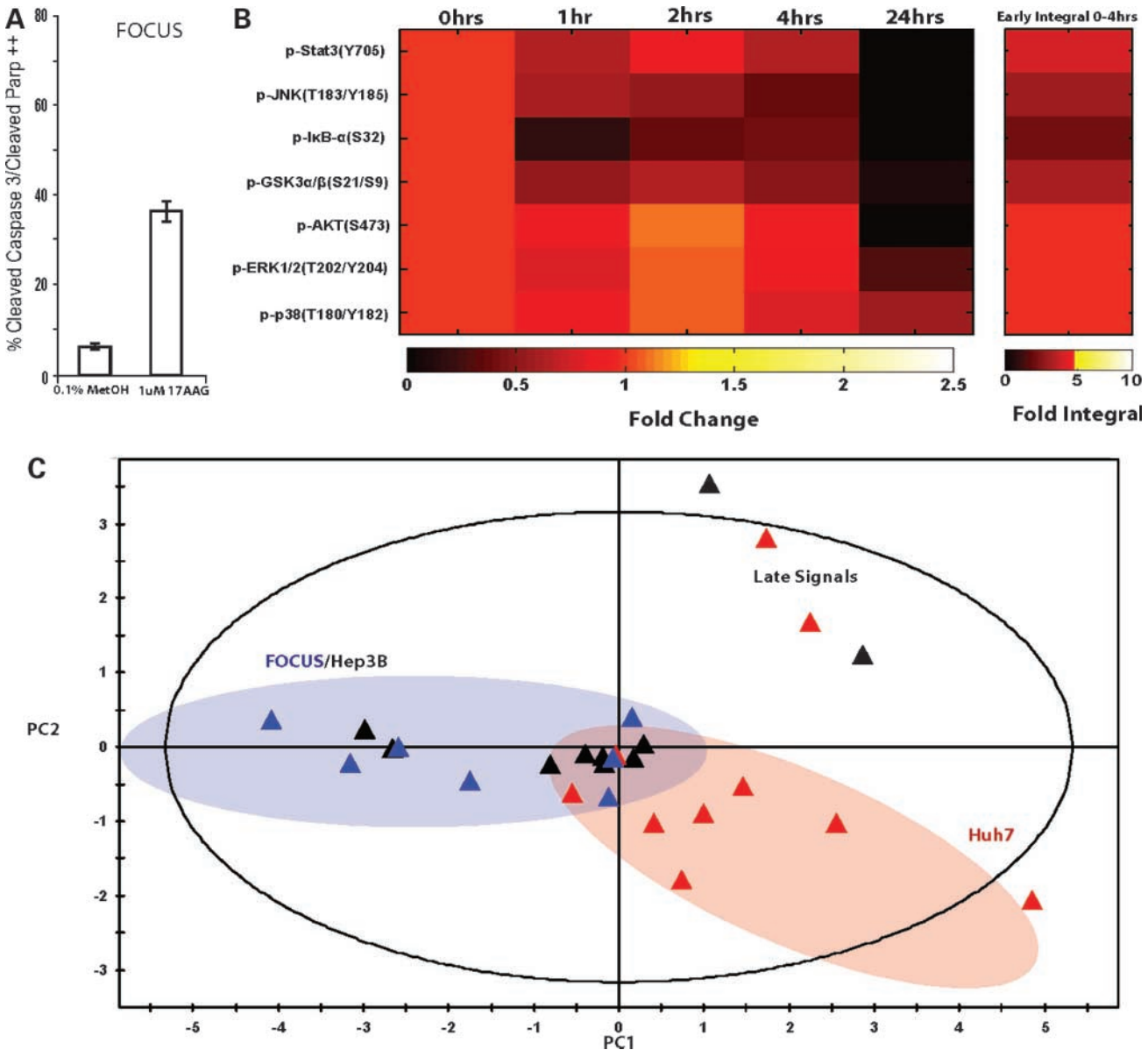

Figure 4. Adding signaling data from another HCC cell line (FOCUS) to the PCA correctly clusters FOCUS cells with sensitive Hep3B cells. **A,** mean of triplicate measurements of the percentage of double-positive FOCUS cells in response to 1 μmol/L 17AAG at 48 h. The gating strategy was the same as in Fig. 1A. **B,** signaling time course of FOCUS cells in response to 1 μmol/L 17AAG. Time point measurements are represented as mean signaling fold change relative to vehicle only controls. **C,** a principal components scores plot, as in Fig. 3, correctly classifies FOCUS cell phosphoprotein signaling measurements as homologous to 17AAG-sensitive Hep3B cells in the two-component model.

Published OnlineFirst August 11, 2009; DOI: 10.1158/1535-7163.MCT-08-1203

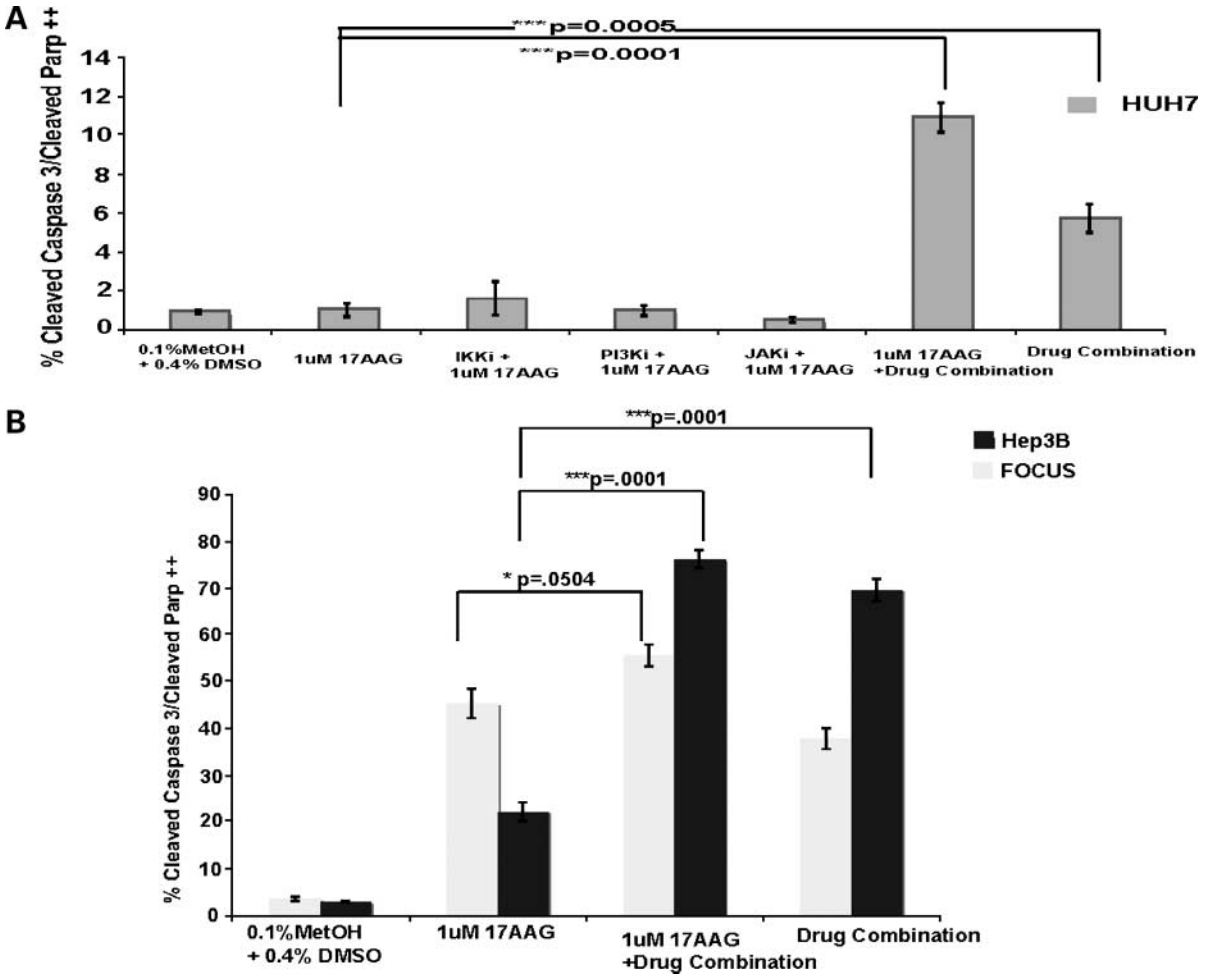

Figure 5. Where inhibition of singular nodes fails, pretreatment with a combination therapy sensitizes Huh7 cells to 17AAG and works as well or better than 17AAG in all cell lines tested. **A,** double-positive populations of Huh7 cells (mean of triplicate ± SE as gated in Fig. 1A) in response to different treatments at 48 h. The IKK inhibitor BMS-345541 was used at 15 μmol/L, the PI3K inhibitor PI103 was used at 5 μmol/L, and the JAK inhibitor JAK inhibitor 1, pyridone 6, was used at 3 μmol/L. The *P* values were obtained by a *t* test. **B,** double-positive populations for the listed treatments of Hep3B and FOCUS cells at 48 h. *Columns,* mean of triplicates; *bars,* SE. The *P* values were obtained by a *t* test. The drug combination is the same as in **A**.

seven canonical kinase signaling effects, phospho-AKT (Ser^{473}), phospho-ERK1/2 (Thr^{202}/Tyr^{204}), phospho-STAT3 (Tyr^{705}), phospho-p38 (Thr^{180}/Tyr^{182}), phospho-JNK (Thr^{183}/Tyr^{185}), phospho–GSK-3α/β (Ser^{21}/Ser^{9}), and phospho–IκB-α (Ser^{32}), with a goal of ascertaining whether a quantitative combination of a particular subset of these signals might be especially critical in clustering the HCC line responses to 17AAG.

We found that a PCA-based model consisting of two principal components explains 91% of the cumulative variance captured by the model. This variation can be classified as early variation (PC1) and late variation (PC2; Fig. 3). All cell lines and signals inhabit the same principal components space, implying that there is a general homology of response. This overall homology stresses that the drug is operating similarly in all cell lines tested and that the phenotypic responses are not likely to be based on the metabolic inactivation of 17AAG or a rapid cellular efflux. The early variation axis (PC1) best separates the cell lines with disparate responses, suggesting that this previously documented early signaling phenomena (17) can be correlated with a cellular phenotype.

The PCA-based visualization accurately maps the sensitive FOCUS cell line to the same region as Hep3B cells (Fig. 4). This greatly improves our confidence that the variation captured in two-dimensional principal components space is relevant to the disparate cell phenotypes and that our analysis has captured important biological information. The success of our PCA mappings suggests that data-driven modeling can effectively reduce the dimensionality of multitarget perturbations and provide a compact, easy-to-interpret analytic method for determining the most phenotypically relevant parameters for further investigations.

Published OnlineFirst August 11, 2009; DOI: 10.1158/1535-7163.MCT-08-1203

Previous data-driven modeling efforts (24, 25) have shown that a systematic signaling analysis of growth factor–induced and cytokine-induced cellular phenotypes captures enough signaling variation that the phenotypic effects of drug perturbations can be predicted a priori. Kumar et al. (18) extended this analysis to show that multiple signals measuring the off-target effects of inhibitors are necessary to predict drug effects on epidermal growth factor–induced migration. Our quantitative analysis of 17AAG leads to testable hypotheses about the targeting of early IKK, PI3K, and JAK-STAT inhibition in 17AAG-induced cell death (Fig. 2). The individual targeted pharmacologic pretreatment of these three survival pathways fails to abrogate the resistance phenotype, but the combined pretreatment is able to synergistically sensitize Huh7 to 17AAG (Fig. 5A). This evidence suggests that cumulative early action of the IKK, PI3K, and JAK-STAT pathway families may be responsible for a portion of the drug resistance phenotype of Huh7.

Although the combination therapy potentiates 17AAG-induced cell death in all cell lines tested, the most striking consequence of our study is the ability of combination therapy alone to recapitulate the cell death effect of 17AAG in a manner that is equal to or greater than the singular effect of 17AAG. This effect has two distinct modalities. In Huh7 and Hep3B cells, the combination treatment works approximately 5- and 3-fold better, respectively, than 17AAG alone. In contrast, the combination treatment is of similar efficacy to 17AAG alone in FOCUS cells (Fig. 5). These distinct modalities can be correlated with the spectrum of multiple drug interactions in the combination therapy (Fig. 6). We speculate that these correlations may suggest a basis for future work on the cell-specific nature of both the proapoptotic/antiapoptotic function of 17AAG and how synergy between nodes may play a role in the efficacy of multidrug combinations and multitarget inhibitors.

By using principal components modeling of a drug perturbation to guide the recreation of a more specific therapeutic strategy, we have shown that we can not only recreate the effect of a multitarget drug but that the recreated effect can work better than the original drug. The

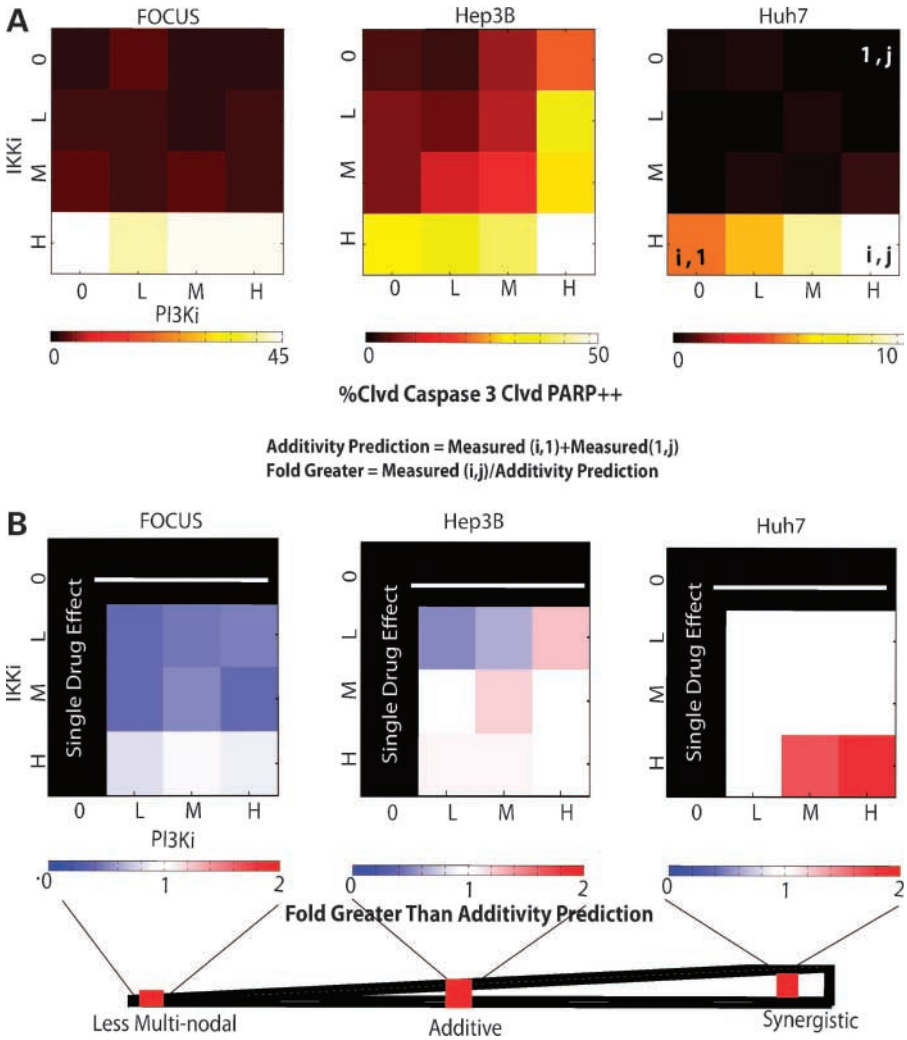

Figure 6. FOCUS, Huh7, and Hep3B cells exhibit different amounts of multinode effects in a JAK inhibitor background. **A,** a matrix of the mean of duplicate measurements of the percentage of double-positive cells in response to varying concentrations of IKK inhibitor (*IKKi*) and PI3K inhibitor (*PI3Ki*) in a JAK (3 μmol/L) inhibitor background. The compounds are the same as in Fig. 4. Concentrations are as follows: IKK inhibitor: high (*H*), 20 μmol/L; medium (*M*), 6.66 μmol/L; low (*L*), 2.22 μmol/L; PI3K inhibitor: high, 5 μmol/L; medium, 1.66 μmol/L; low, 0.55 μmol/L. **B,** the synergy plots display the fold deviation from predictions based on the assumption of additivity. Briefly, additivity predictions for any double-drugged entry (*i,j*) were calculated by adding the ith row of the first column (i.e., the singular IKK effect at that concentration) to the first row, jth column (i.e., the singular PI3K effect at that concentration). Then, the measured value at the double-drugged entry (*i,j*) was divided by the additivity prediction. This created a metric that describes synergy versus additivity.

Published OnlineFirst August 11, 2009; DOI: 10.1158/1535-7163.MCT-08-1203

existence of differences in the multidrug interactions (Fig. 6) underscores the value of recreating multitarget effects. In decoupling the effects from the context of 17AAG, we find that the potential exists to allow for the individual adjustment of the elements of a combination therapy.

Our suggestion that a specified combination therapy may produce a less generally pleiotropic effect than the multitarget compound from which it has been rebuilt arises from comparative consideration of the diversity of the cellular effects of the initial multitarget compound along with the off-target effects of the combination therapy. In our particular case, which is certainly a fairly extreme example, Hsp90 in *S. cerevisiae* is known to interact with ~10% of the open reading frames examined in a recent study (7). Although a similar analysis is not available for the three compounds of our combination therapy, it seems plausible that our combination therapy is less broadly cross-reactive for several reasons. A systematic study of 317 kinases found that for PI103, ~10 cellular kinases had IC_{50}s of <10 μmol/L *in vitro* (26). BMS-345541 is an allosteric inhibitor of IKK and failed to significantly inhibit a panel of 15 related kinases at concentrations as high as 100 μmol/L (27). Our Janus kinase inhibitor, pyridone 6, although less well tested than the other two, fails to inhibit the proliferation of cell lines that do not harbor activated JAK-STAT signaling (28). Thus, in spite of the inevitable existence of some off-target effects, it seems highly unlikely that the magnitude of these effects could approach the pleiotropy of 17AAG. Therefore, the generalizability of this approach to other forms of multitarget compounds will likely prove increasingly practical as more specific inhibitors become available.

Disclosure of Potential Conflicts of Interest

No potential conflicts of interest were disclosed.

Acknowledgments

We thank Hyung-Do Kim and Luke Gilbert for insightful discussions and Pam Kreeger, Megan Palmer, Shannon Alford, Shan Wu, Matt Lazzara, and Arthur Goldsipe for excellent technical input.

References

1. Lynch TJ, Bell DW, Sordella R, et al. Activating mutations in the epidermal growth factor receptor underlying responsiveness of non-small-cell lung cancer to gefitinib. N Engl J Med 2004;350:2129–39.

2. Chabner BA, Roberts TG, Jr. Chemotherapy and the war on cancer. Nat Rev Cancer 2005;5:65–71.

3. Petrelli A, Giordano S. From single to multi-target drugs in cancer therapy: when aspecificity becomes an advantage. Curr Med Chem 2008;15:422–32.

4. Uehara Y, Makoto H, Tomio T, Umezawa H. Phenotypic change from transformed to normal induced by benzoquinonoid ansamycins accompanies inactivation of p60src in rat kidney cells infected with Rous sarcoma virus. Mol Cell Biol 1986;6:2198–206.

5. Whitesell L, Lindquist S. Hsp90 and the chaperoning of cancer. Nat Rev Cancer 2005;5:761–72.

6. Whitesell L, Shifrin SD, Schwab G, Neckers L. Benzoquinonoid ansamycins possess selective tumoricidal activity unrelated to src kinase inhibition. Cancer Res 1992;52:1721–8.

7. Zhao R, Davey M, Hsu YC, et al. Navigating the chaperone network: an integrative map of physical and genetic interactions mediated by the Hsp90 chaperone. Cell 2005;120:715–27.

8. Kamal A, Thao L, Sensintaffar J, et al. A high-affinity conformation of Hsp90 confers tumour selectivity on Hsp90 inhibitors. Nature 2003;425:407–10.

9. Hostein I, Robertson D, DiStefano F, et al. Inhibition of signal transduction by the Hsp90 inhibitor 17-allylamino-17-demethoxygeldanamycin results in cytostasis and apoptosis. Cancer Res 2001;61:4003–9.

10. Bareng J, Jilani I, Gorre M, et al. A potential role for Hsp90 inhibitors in the treatment of Jak2 mutant-positive diseases as demonstrated using quantitative flow cytometry. Leuk Lymphoma 2007;48:2189–95.

11. Mitsiades CS, Mitsiades NS, McMullan CJ, et al. Antimyeloma activity of heat shock protein-90 inhibition. Blood 2006;107:1092–100.

12. Garcia-Morales P, Carrasco-Garcia E, Ruiz-Rico P, et al. Inhibition of Hsp90 function by ansamycins causes downregulation of cdc2 and cdc25c and G_2/M arrest in glioblastoma cell lines. Oncogene 2007;26:7185–93.

13. Solit DB, Ivy SP, Kopli C, et al. Phase 1 trial of 17-allyamino-17-demethoxygeldanamycin in patients with advanced cancer. Clin Cancer Res 2007;13:1775–82.

14. Chandarlapaty S, Sawai A, Qing Y, et al. SNX2112, a synthetic heat shock protein 90 inhibitor, has potent antitumor activity against HER kinase-dependent cancers. Clin Cancer Res 2008;14:240–8.

15. Yun BG, Matts R. Hsp90 functions to balance the phosphorylation state of Akt during C2C12 myoblast differentiation. Cell Signal 2005;17:1477–85.

16. Donze O, Abbas-Terki T, Picard D. The Hsp90 chaperone is both a facilitator and a repressor of the dsRNA-dependent kinase PKR. EMBO J 2001;20:3771–80.

17. Koga F, Xu W, Karpova TS, et al. Hsp90 inhibition transiently activates Src and promotes Src-dependent Akt and Erk activation. Proc Natl Acad Sci U S A 2006;103:11318–22.

18. Kumar N, Afeyan R, Kim HD, Lauffenburger DA. A multi-pathway model enables prediction of kinase inhibitor cross-talk effects on migration of Her2-overexpressing mammary epithelial cells. Mol Pharmacol 2008;73:1668–78.

19. Janes KA, Yaffe MB. Data-driven modeling of signal-transduction networks. Nat Rev Mol Cell Biol 2006;7:820–8.

20. Lee HC, Tian B, Sedivy J, Wands JR, Kim M. Loss of Raf kinase inhibitor protein promotes cell proliferation and migration of human hepatoma cells. Gastroenterol 2006;131:1208–17.

21. Jolliffe IT. Principal components analysis. 2nd ed. New York: Springer-Verlag; 2002.

22. Eriksson L, Johansson E, Kettanel N, Wold S. Multi- and megavariate data analysis, principles and applications. Umeå (Sweden): Umetrics AB; 2001.

23. Mardia KV, Kent JT, Bibby JM. Multivariate analysis. New York: Academic Press; 1979.

24. Miller-Jensen K, Janes KA, Brugge JS, Lauffenburger DA. Common effector processing mediates cell-specific responses to stimuli. Nature 2007;448:604–8.

25. Kemp ML, Wille L, Lewis CL, Nicholson LB, Lauffenburger DA. Quantitative network signal combinations downstream of TCR activation can predict IL-2 production response. J Immunol 2007;178:4984–92.

26. Karaman MW, Herrgard S, Treiber DK, et al. A quantitative analysis of kinase inhibitor selectivity. Nat Biotechnol 2008;26:127–32.

27. Karin M, Yamamoto Y, Wang QM. The IKK NF-κB system: a treasure trove for drug development. Nat Rev Drug Discov 2004;3:17–26.

28. Pedranzini L, Dechow T, Berishaj M, et al. Pyridone 6, a pan-Janus-activated kinase inhibitor, induces growth inhibition of multiple myeloma cells. Cancer Res 2006;66:9714–21.

Published OnlineFirst August 11, 2009; DOI: 10.1158/1535-7163.MCT-08-1203

Molecular Cancer Therapeutics

Three-kinase inhibitor combination recreates multipathway effects of a geldanamycin analogue on hepatocellular carcinoma cell death

Justin R. Pritchard, Benjamin D. Cosgrove, Michael T. Hemann, et al.

Mol Cancer Ther 2009;8:2183-2192. Published OnlineFirst August 11, 2009.